Heliyon 6 (2020) e05681

Contents lists available at ScienceDirect

Heliyon

journal homepage: www.cell.com/heliyon

Research article

Investigation on penetration of saffron components through lipid bilayer bound to spike protein of SARS-CoV-2 using steered molecular dynamics simulation

Azadeh Kordzadeh [a], Ahmad Ramazani Saadatabadi [a,*], Amin Hadi [b,**]

[a] Chemial and Petroleum Egineering Department, Sharif University of Technology, Tehran, Iran
[b] Cellular and Molecular Research Center, School of Medicine, Yasuj University of Medical Sciences, Yasuj, Iran

ARTICLE INFO

Keywords:
SARS-CoV-2
Molecular dynamics simulation
Crocin
Crocetin
Safranal
Picrocrocin
Bioinformatics
Biomedical engineering
Biotechnology
Molecular biology
Proteins

ABSTRACT

A coronavirus identified as COVID-19 is the reason for an infection outbreak which is started in December 2019. NO completely effective drugs and treatments are not recognized for this virus. Recently, saffron and its compounds were used to treat different viral diseases. Saffron extract and its major ingredients have shown antiviral effects. In this study, the steered molecular dynamics simulation was used for investigating the effect of four main components of saffron that include: crocin, crocetin, safranal, and picrocrocin as candidate for drug molecules, on COVID-19. The binding energies between drug molecules and spike protein and the main protease of the virus were evaluated. The obtained results based on Lennard-Jones and electrostatic potentials demonstrated that crocetin has a high affinity towards spike protein and also the main protease of the virus. Also, the quantum mechanics calculations elucidated that the crocetin could overcome energy barrier of lipid bilayer with strong dipole moment and polarizability. The pharmacokinetic and ADMET properties proved that crocetin could be a suitable drug candidate. So, crocetin could be a promising drug for treatment of COVID-19.

1. Introduction

A coronavirus (CoV), named as 2019 novel coronavirus (COVID-19), is believed that is the responsible agent for the pandemic that commenced in Wuhan, China, in December 2019 [1]. This virus could infect humans and probably many other animal species, with symptoms like dry cough, sore throat, nasal congestion, tiredness, fever, loss of taste, and smell similar to Severe Acute Respiratory Syndrome(SARS) and Middle East Respiratory Syndrome (MERS) [2].

There are four categories for CoVs: Alphacoronavirus, Betacoronavirus (which primarily infect mammals), Gammacoronavirus, and Deltacoronavirus (which primarily infect birds) [3,4]. By the end of 2019, six kinds of human CoV have been recognized: HCoV-NL63, HCoV-229E, belonging to Alphacoronavirus genera, HCoV-OC43, HCoVHKU1, SARS-CoV, and MERS-CoV, belonging to Betacoronavirus genera [5]. The severe acute respiratory syndrome 2 (SARS-CoV-2) caused the outbreak of epidemics at the beginning of the 21st century. The COVID-19 which is classified as Betacoronavirus was the seventh type of human coronavirus. The origins of the CoVs are still unknown, however, increasing evidence demonstrates a link between the COVID-19 and other similar known coronaviruses circulating in bats [6]. Phylogenetic studies revealed that two SARS-CoV-2 sequences isolated from bats in 2015 and 2017 are very similar to the COVID-19 [7].

According to the World Health Organization (WHO), on August 8, 2020, 716075 confirmed deaths have been recorded due to COVID-19 [8]. At present, effective treatment options for COVID-19 remain very limited. Many researchers are trying to find an effective treatment for SARS-CoV-2. Some studies tried to clarify the mechanism of attachment of virus to human cells [9,10]. Figure 1 shows a general schematic of SARS-CoV-2 and its structural proteins. The four structural proteins of βcoronavirus are membrane (M), envelope (E), spike (S), and nucleocapsid (N) protein, mediation of coronavirus host infection is established by spike (S) protein. An investigation by scientists in China revealed that the SARS-CoV-2 requires angiotensin-converting enzyme 2 (ACE2) receptor for their binding and invasion of the host [11,12].

Computational methods could be efficient methods in the drug discovery field which decrease the required time and budget for the

* Corresponding author.
** Corresponding author.
E-mail addresses: ramazani@sharif.edu (A. Ramazani Saadatabadi), amin.hadi@yums.ac.ir (A. Hadi).

https://doi.org/10.1016/j.heliyon.2020.e05681
Received 17 October 2020; Received in revised form 19 November 2020; Accepted 3 December 2020

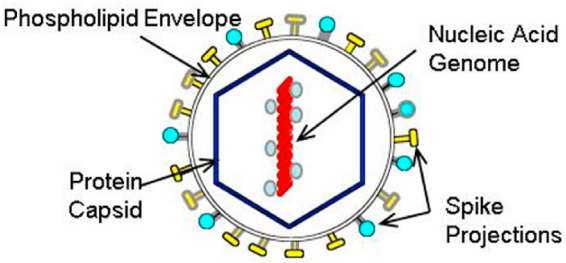

Figure 1. Schematic representation of SARS-Cov-2 and its structural proteins [46].

discovery of a new drug. Methods such as molecular docking and molecular dynamics simulation widely used for investigating COVID-19 [13,14,15,16]. Elficky [17,18] by using molecular docking explained that anti-hepatitis C virus drugs such as Sofosbuvir, Ribavirin, and Remidisivir have high binding energy towards the main protease of SARS-CoV-2. Sethi et al. [19] by molecular docking indicated that the gelatine could be a candidate for blocking spike protein of SARS-CoV-2. Bzowka et al. [20] by using molecular dynamics simulation elucidated that despite a high level of sequence similarity between the main protease of SARS-Cov-2 and SARS, the active sites in both proteins show major differences in both shape and size indicating that repurposing SARS drugs for COVID-19 may be futile. Aanouz et al. [21] examined the Moroccan medical plants as inhibitors for SARS-CoV-2. The binding energy between 64 herbal extracts and main protease of SARS-CoV-2 was calculated by molecular docking. Three molecules (Crocin, Digitoxigenin, and b-Eudesmol) are proposed as inhibitors against the coronavirus based on the energy types of interaction between these molecules and studied protein. However, the introduction of a new drug required further investigation such as ADMET (absorption, distribution, metabolism, excretion and toxicity) parameters. Lipinski introduced the 'Rule of 5' (Ro5) as a criterion for evaluation the drug-likeness of molecules. The rule explains that compounds have poor absorptivity and bioavailability if their molecular weight is >500 g/mol, hydrogen bond donors>5, hydrogen bond acceptors>10 and log P > 5 [22,23].

The molecular docking method and molecular dynamics (MD) simulations could determine the binding energy between ligand and receptor. The molecular docking is an efficient method that could analyse a large number of ligands but the ignorance dynamic of ligand and receptor decreases the accuracy of this method [24]. The molecular dynamics simulation is an accurate method but it is computationally expensive with limit number of studied molecules [25]. Finding an efficient and accurate computational method is valuable. The steered molecular dynamics (SMD) [26,27] have developed and applied to study the mechanical unfolding of biomolecules [28,29], transportation of ions [30,31], and organic compounds through membrane channels [32,33]. This method is also employed to probe unbinding pathways of the ligand from its receptor [34,35]. SMD was used for finding drug molecules for blocking influenza virus receptors [36,37,38]. SMD is shown to be as powerful as the molecular mechanics/Poisson-Boltzmann (Generalized Born) surface area (MM/PB(GB)SA) MM-PBSA method [39,40] in predicting binding affinity but about one order of magnitude faster.

Some plant compounds, such as saffron, have shown antiviral properties. Saffron (Crocus sativus) is a plant from the genus Iridaceae with many properties, including medicinal and food colouring. The main components of saffron are Crocin, Picrocrocin, Crocetin, and Safranal, which are shown in Figure 2. The mass faction of each component in saffron varies according to the geographical area and indicate the quality of saffron. Much research has been carried out on the anti-tumor and antiviral properties of saffron. All contributing not only to the sensory profile of saffron colour, taste, and aroma, but also to the health-promoting properties [41]. Crocin quickly dissolves in water with typically deep red in colour. In addition to being an excellent colorant, Crocin also acts as an antioxidant by quenching free radicals, protecting cells and tissues against oxidation. Picrocrocin and Safranal are the main responsible agents for the aroma and taste of saffron, respectively [42]. Antiproliferation and cytotoxicity on tumor cells are anti-cancer functions of Crocetin. It is proved that saffron components positively correlate with a lower risk of diseases including metabolic disorders (gastric disorder), premenstrual syndrome, depression, insomnia and anxiety, cardiovascular disease, as well as many types of cancers [43]. Much research has been carried out on the anti-tumor and antiviral properties of saffron. Soleimani et al. [44] investigated the anti-HSV-1 and anti-HIV-1 effects of Iranian saffron and its main constituent's in-vitro, including Crocin and Picrocrocin. Their research revealed that the aqueous saffron extract had a mild activity against HIV-1 and HSV-1; however, crocin and picrocrocin had an effective antiviral activity. In this study, these two herbal medicines prevented the virus from entering the Vero cell, which disrupted the virus entry mechanism. Escribano et al. [45] indicated that saffron compounds inhibit the growth of cancer cells.

Our search in literature indicates that the SMD simulation between spike protein of SARS-CoV-2 and drugs has not been addressed in

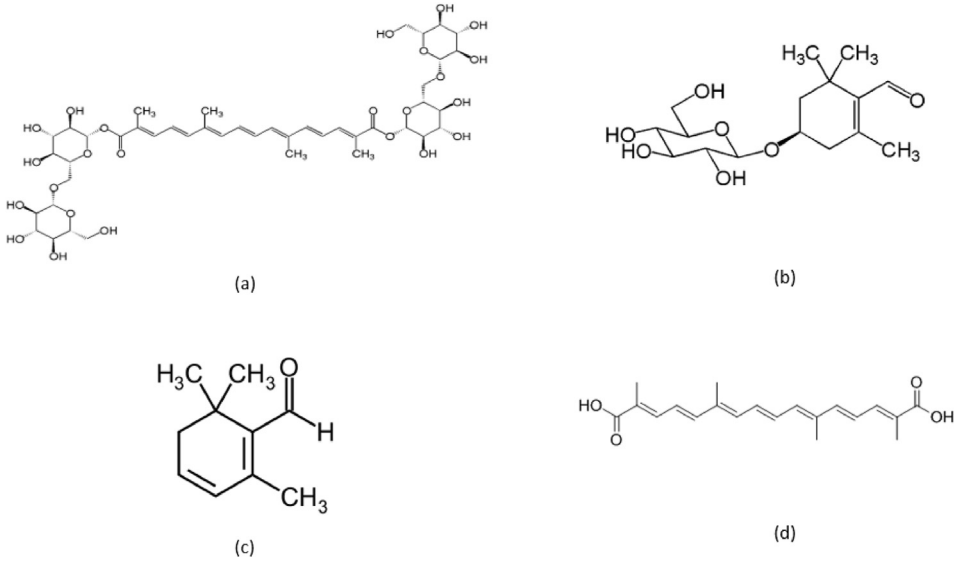

Figure 2. The chemical structure of (a) crocin, (b) picrocrocin, (c) safranal and (d) crocetin [47].

Table 1. Pharmacokinetic and toxicological parameters of crocin, crocetin, picrocrocin and safranal.

Compounds	Crocin	Crocetin	Picrocrocin	safranal
HBD[a]	14	2	4	0
HBA[b]	24	4	7	1
MW[c]	976	328.40	330.37	150.22
Log P[d]	4.70	4.21	0.03	2.30
Mutagenic	No	No	No	No
Tumorigenic	No	No	No	No
Irritant	No	No	Yes	Yes
Drug likeness	-1.85	1.24	-6.9	-4.39
Drug score	0.28	0.56	0.28	0.29

[a] Number oh hydrogen bond donor.
[b] Number oh hydrogen bond acceptor.
[c] Molecular weight.
[d] Octanol/water partition coefficient.

Table 2. Energies (Hartree) of HOMO, LUMO and band gap, dipole moment (Debye), polarizability (Bohr) for crocin, crocetin, picrocrocin and safranal.

Compounds	crocetin	Crocin	picrocrocin	Safranal
HUMO	-0.10267	-0.10838	-0.05716	-0.06679
LUMO	-0.19295	-0.18368	-0.24184	-0.22576
Band gap	0.09028	0.0753	0.18468	0.15897
Dipole moment	5.05	3.34	3.36	3.83
a_{xx}	1831.620	1922.435	267.518	177.513
a_{yy}	293.484	620.720	230.203	167.359
a_{zz}	130.933	388.517	244.934	93.107
Exact polarizability	2256.037	2931.672	742.655	437.979

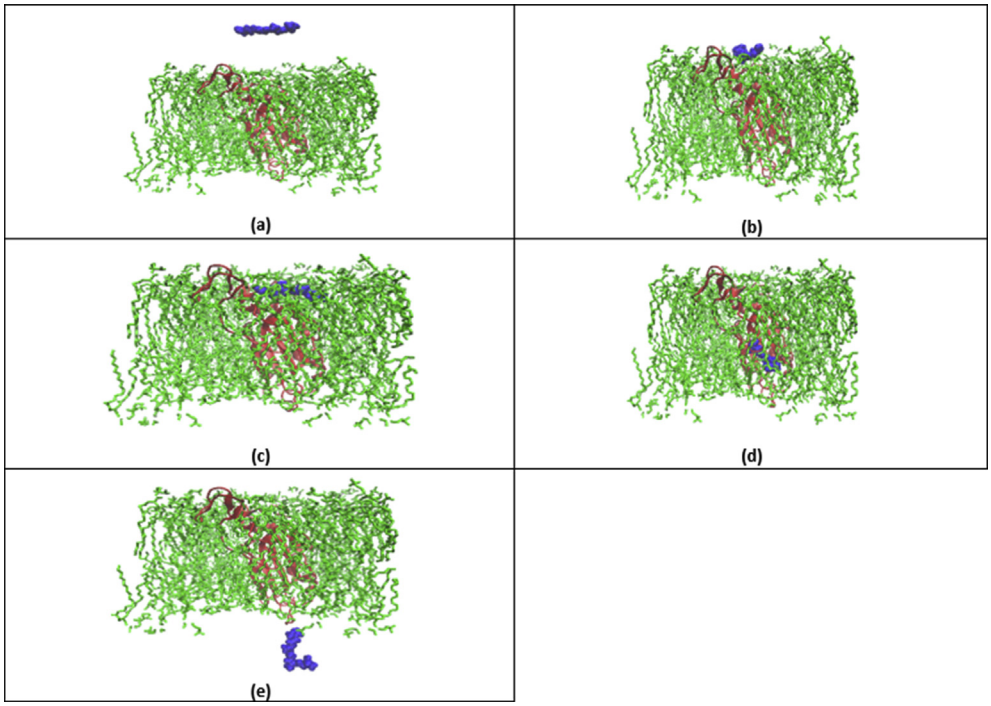

Figure 3. Snapshots of the crocetin molecule penetration through the lipid bilayer, (a) 0 nm, (b) 2 nm, (c) 4 nm, (d) 6 nm, (e) 8 nm displacement of crocetin molecule. The red cartoon, blue vdW sphere and green lines show the spike protein (PDB ID = 6M0J), crocetin molecule and DPPC bilayer, respectively. The water molecules are ignored for clarification. See also video S1 in Supplementary Information.

previous researches and need a thorough and comprehensive investigation which could be used for future drug and treatment discovery. So in this study by using SMD simulation method the penetration of saffron's main components that include: Crocin, Crocetin, Picrocrocin, and Safranal, through spike protein of SARS-CoV-2 embedded in dipalmitoylphosphatidylcholine (DPPC) lipid bilayer was simulated. In the next

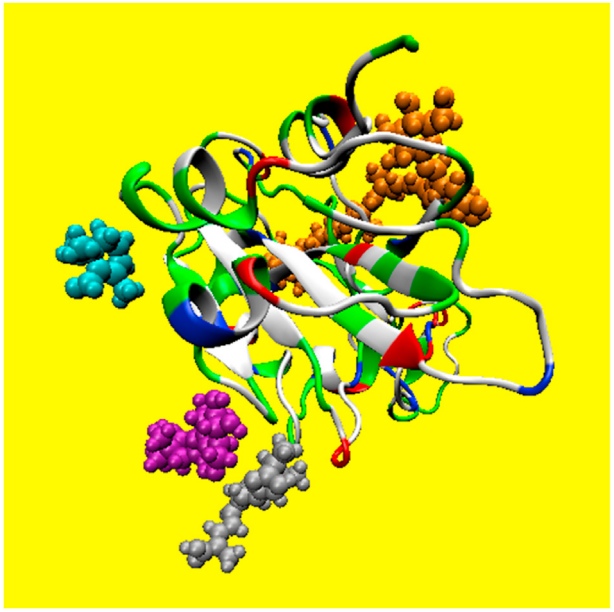

Figure 4. The interaction site of drug molecules with spike protein (PDBID = 6M0J) at entrance of lipid bilayer. The orange, cyan, magenta and silver vdW spheres show the crocin, safranal picrocrocin and crocetin drug molecules, respectively. The spike protein is shown with white, green, red and blue cartoon which represent nonpolar, polar, acidic and basic amino acids, respectively.

step, the binding affinity between main component of saffron and the main protease of SARS-CoV-2 was evaluated. By considering the spike protein and the main protease of SARS-CoV-2 a complete representation of the virus was simulated.

2. Model and method

2.1. The structural model

The Crocin, Crocetin, Picrocrocin, and Safranal molecules were selected as drug molecules. The initial structure of drug molecules was obtained from DRUGBANK server [48]. The structure of spike protein (PDB ID 6M0J) and main protease (PDB ID 6M03) of SARS-CoV-2 were obtained from protein data bank server [49]. For constructing an embedded lipid bilayer with spike protein, at first an equilibrated 128 Dipalmitoylphosphatidylcholine (DPPC) lipid bilayer was constructed with CHARMM-GUI server [50]. Then the spike protein was embedded in lipid bilayer, in this step 6 lipid molecules (3 lipid molecules from each leaflet) were removed. The embedded lipid bilayer equilibrated in 28 steps until the area per lipid reached to 64.0 $Å^2$ which is close to experimental value [51]. Finally, a 122 DPPC lipid bilayer with embedded spike protein was obtained.

2.2. Force field

The GROMACS 5.1.4 simulation package [52] was employed to perform all simulations. The visual molecular dynamics (VMD 1.9.1) [53] program was used for molecular visualization. The all-atom GROMOS54A7 force field was employed to calculate all bonded and nonbonded interactions [54]. The simple point charge [55] model was selected for water molecules. Topology files of drug molecules were obtained by using PRODRG server [56] and the partial charges are to be corrected by performing the corresponding quantum mechanics QM calculations. Quantum mechanics (QM) calculations performed by using GAMESS [57] software by employing DFT, 6-31G(d,p), B3LYP method [58,59], along with monitoring variation of molecular configuration to achieve minimum energy of molecule. The partial charges of the atoms were calculated by using electrostatic potential method (ESP) [60] and by considering the fact that, the molecules are present in water medium.

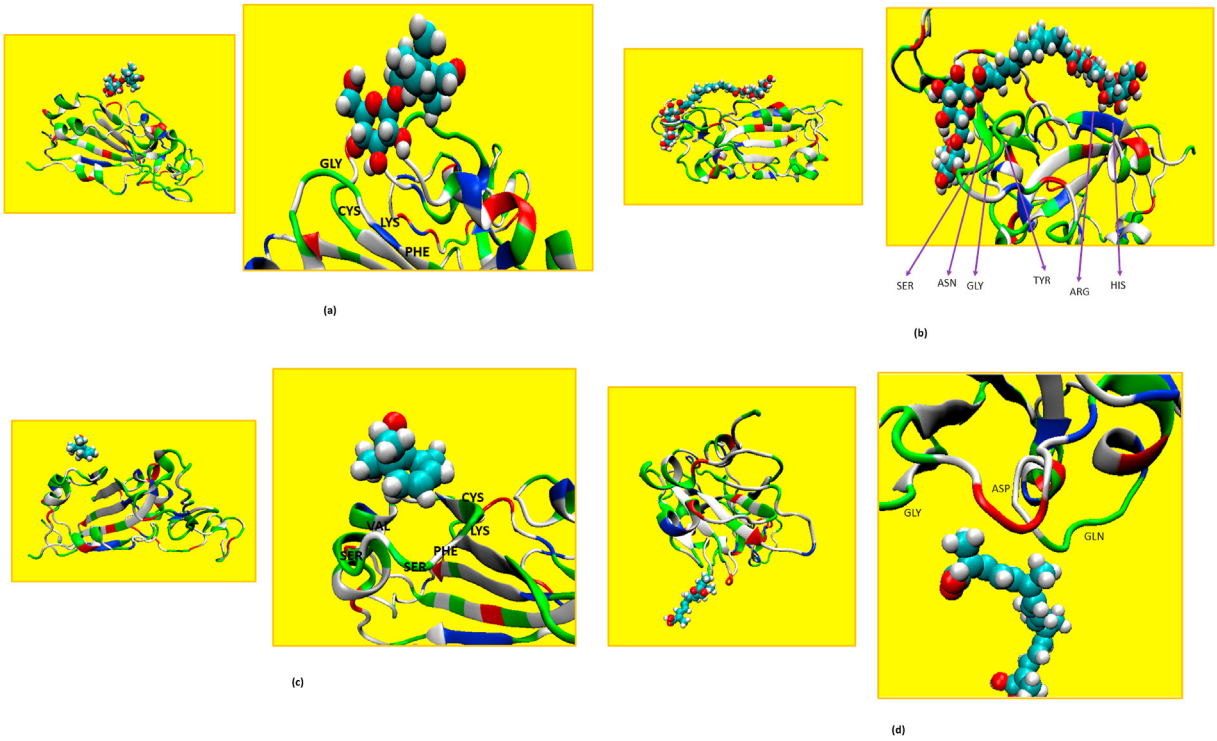

Figure 5. The interaction site of (a) picrocrocin, (b) crocin, (c) safranal and (d) crocetin with spike protein (PDBID = 6M0J) at entrance of lipid bilayer. The cyan, white and red vdW spheres show the carbon, hydrogen and oxygen atoms in drug molecules, respectively. The spike protein is shown with white, green, red and blue cartoon which represent nonpolar, polar, acidic and basic amino acids, respectively.

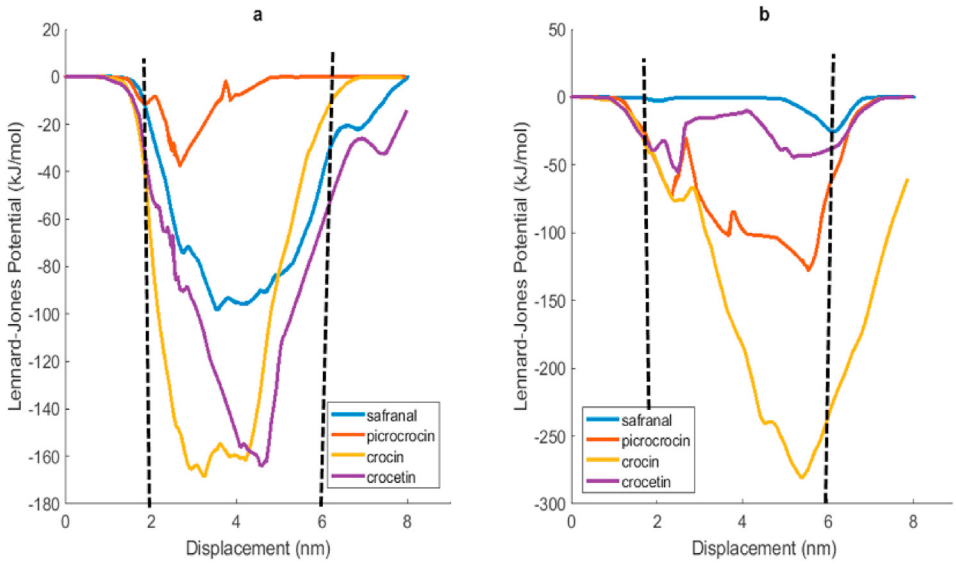

Figure 6. Lennard-Jones (LJ) potential energy profiles between (a) the spike protein (PDB ID = 6M0J) and (b) DPPC bilayer and drug molecules versus displacement drug molecules. The dash lines show the lipid bilayer region.

The pharmacokinetic and toxicological parameters of compounds were obtained by SwissADME server [61].

2.3. MD simulation

The simulations were run in the NPT ensemble. During the simulation the temperature was kept constant at 310 K (physiological temperature) using a Nose'-Hoover thermostat [62] and the pressure was kept constant at 1 bar using the Parrinello–Rahman barostat [63] with semi-isotropic pressure coupling [64]. The time step was 2fs, and the LINCS algorithm [65] was used to constrain all bonds. The long-range electrostatic interaction was calculated with the particle mesh Ewald method with a cut off radius of 1.2 nm [66]. The Lennard-Jones potential was used to calculate the van der Waals (vdW) interaction with a cut off radius of 1.2 nm as recommended [67]. The simulation box dimensions for lipid bilayer and main protease system was ($6.5 \times 6.5 \times 10$ nm^3) and ($12 \times 8 \times 8$ nm^3), respectively. The spike protein embedded in DPPC lipid bilayer was equilibrated for 100 ns, area per lipid was calculated and a value of 64.0 A was obtained, which is in agreement with the experimental measurements [51]. For investigation the interaction of drug molecules with lipid bilayer at first, the drug molecules were initially positioned at a distance of 4 nm from the center of mass of DPPC lipid bilayer. For simulation of main protease, the drug molecules initially were positioned at a distance of 5 nm from the center of mass of the main protease. Then, the energy was minimized using the steepest descent method. The NVT simulation for 5 ns was performed and temperature was set at 310 K. The pressure was adjusted at 1 bar in NPT ensemble for 10 ns. Then the constant velocity SMD was performed. In SMD simulation, the drug

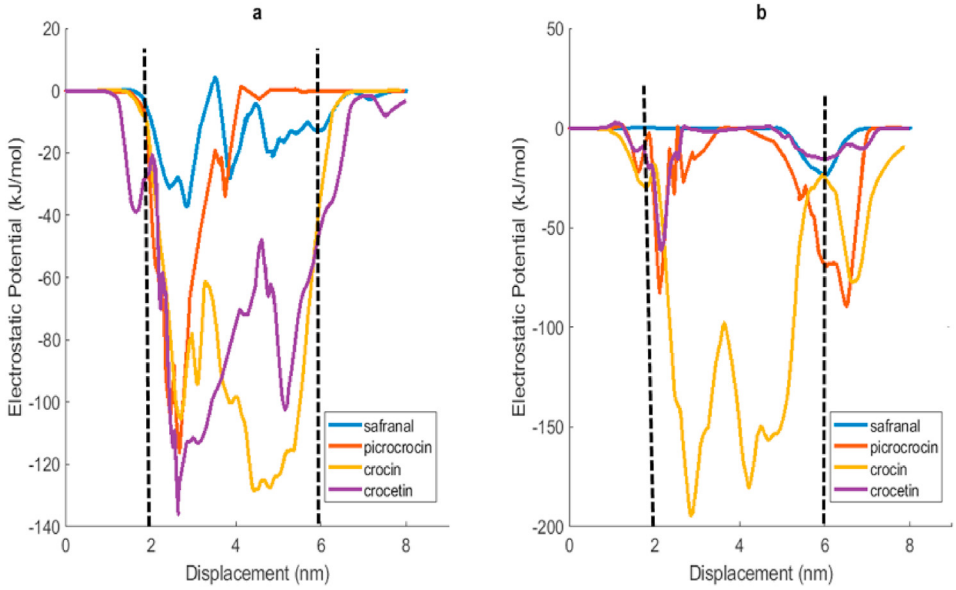

Figure 7. Electrostatic potential energy profiles between (a) the spike protein (PDB ID = 6M0J) and (b) DPPC bilayer and drug molecules versus displacement drug molecules. The dash lines show the lipid bilayer region.

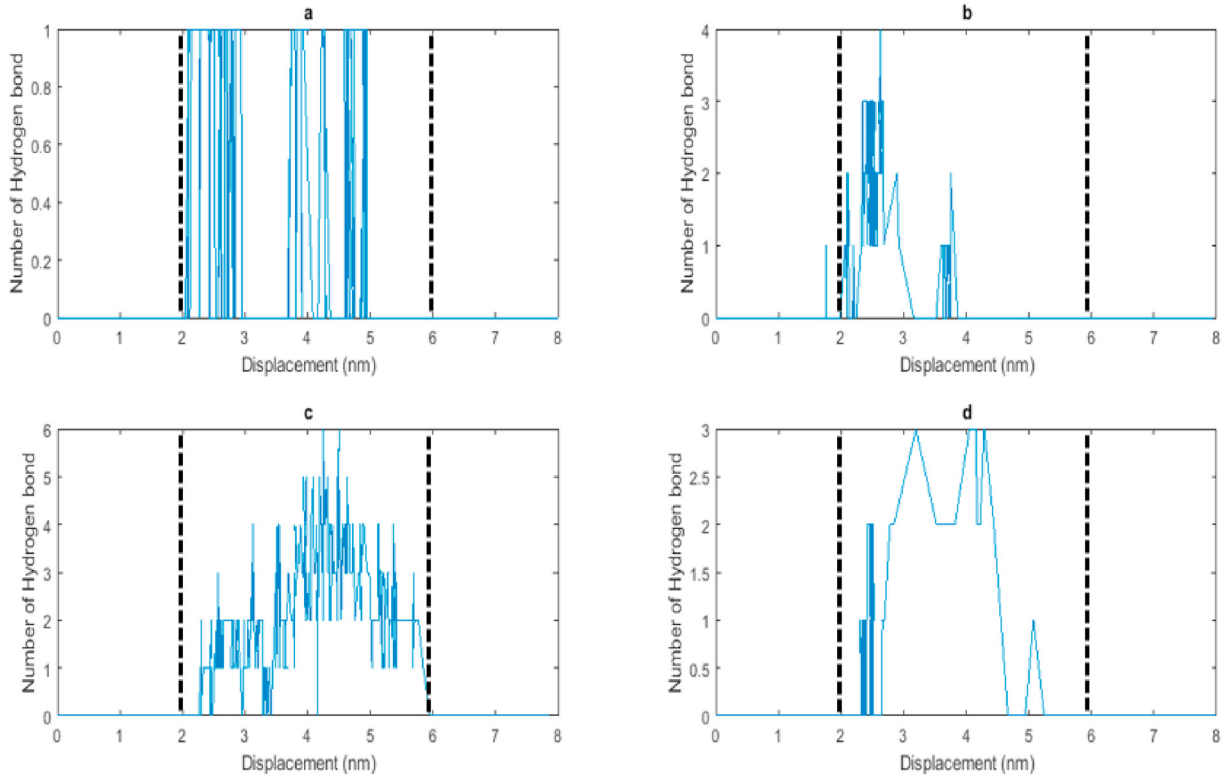

Figure 8. Number of hydrogen bonds between (a) safranal, (b) picrocrocin, (c) crocin and (d) crocetin molecule and spike protein versus displacement drug molecules. The dash lines show the lipid bilayer region.

molecule was attached to dummy atoms via a virtual spring and were moved at a constant velocity. The force needed for the displacement of the dummy atoms to an imaginary point can be calculated by the following equations [27]:

$$F = -\nabla U \tag{1}$$

$$U = k[vt - (r - r_0).n]^2 \tag{2}$$

Where ∇U is the potential energy gradient, k is the spring force constant which is, v is the velocity of pulling, t is the current time, r is the instantaneous vector position, r_0 is the initial vector position of the SMD atom and n is the vector direction which the dummy atom is pulled. In the SMD simulation of the present work, pulling velocities (v) 0.01 $\frac{nm}{ps}$.

3. Results and discussion

3.1. Toxicity analysis and drug score

The pharmacokinetic and toxicological parameters of crocin, crocetin, picrocrocin and safranal are shown in Table 1. Crocin violated three rules of Lipinski of five based on its number of hydrogen bond donors and acceptors and molecular weight. Picrocrocin with 7 hydrogen bond acceptors violated one rule of Lipinski's rule. Safranal and crocetin did not violate any Rule of five. All compound did not have mutagenic and tumorigenic properties. Although, picrocrocin and safranal could be irritant. Comparison of drug score demonstrated that crocin, picrocrocin and safranal have the same drug score while the crocetin with higher drug score could be a suitable candidate as drug molecule.

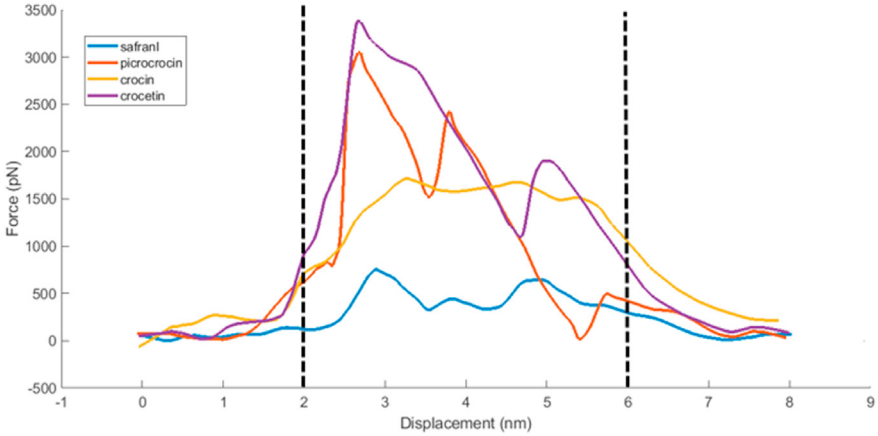

Figure 9. The force-displacement profile of drug molecules during translocation from lipid bilayer. The dash lines show the lipid bilayer region.

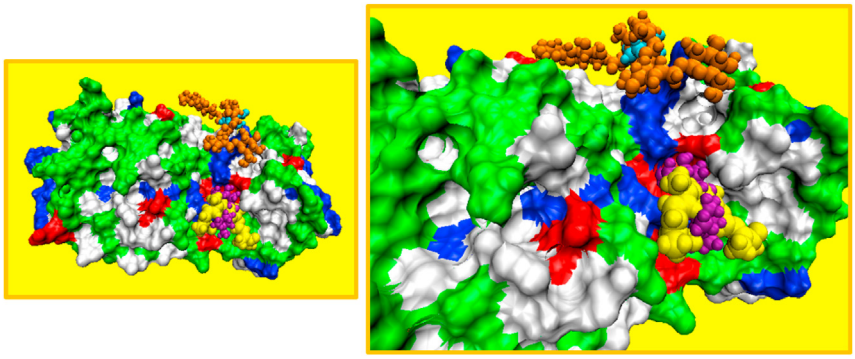

Figure 10. The interaction site of drug molecules with main protease (PDBID = 6M03) at entrance of lipid bilayer. The orange, cyan, magenta and yellow vdW spheres show the crocin, safranal picrocrocin and crocetin drug molecules, respectively. The spike protein is shown with white, green, red and blue surf which represent nonpolar, polar, acidic and basic amino acids, respectively.

3.2. Quantum chemical calculations

For investigating the electronic properties of saffron components the QM calculations was performed as described in section2–3. The obtained results of quantum chemical calculations are represented in Table 2. The energies of highest occupied molecular orbital (HOMO), lowest unoccupied molecular orbitals (LUMO) and the band gap were calculated and molecular orbitals are shown in Figure S1 in Electronic Supplementary information (ESI). Comparison between polarizability and band gap values reveals that with increasing band gap the polarizability decreased. The direction of dipole moment vectors for drug molecules are shown in Figure S1. The magnitude and direction of dipole moment vectors are shown in Figure S2. Considering obtained results, it is evident that crocetin has a strong dipole moment which is different from the other three drug molecules.

3.3. Binding to spike protein

The translocation of the crocetin drug molecule through lipid bilayer is illustrated in Figure 3 (see also Video S1). At first the drug molecule was placed at a distance of 4 nm from the center of mass of the lipid bilayer (Figure 3 (a)). The drug molecule was pulled towards lipid bilayer with a velocity of 0.01 $\frac{nm}{ps}$ and a spring constant of 10 $\frac{kJ}{mol\ A^{-2}}$. Then the drug molecule reached the lipid bilayer surface (Figure 3 (b)) and drug molecule passed the lipid bilayer via spike protein. The translocation of safranal, picrocrocin and crocin drug molecules are shown in Figure. S3, Figure. S4 and Figure. S5, respectively (see also Videos S2, S3 and S4). During passing the crocin molecule from the lipid bilayer, a concave shape was observed in upper leaflet of lipid bilayer (Figure. S5 (d)) and when the crocin molecule exited the bilayer one lipid molecule was extracted.

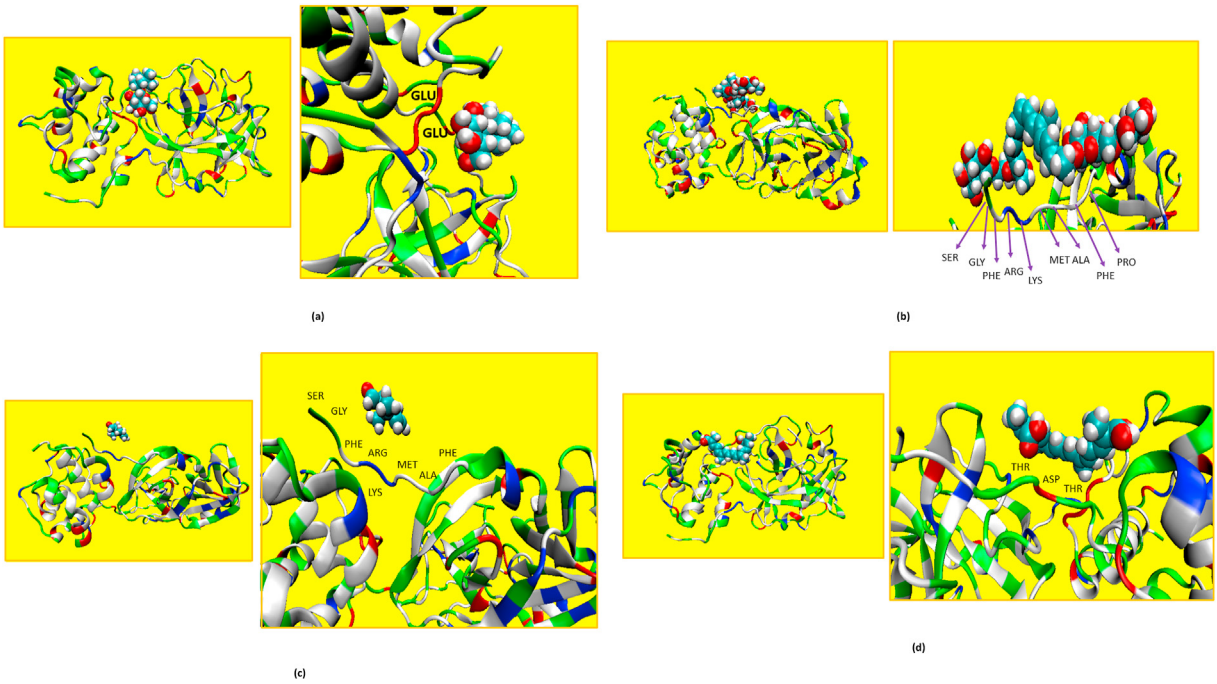

Figure 11. The interaction site of (a) picrocrocin, (b) crocin, (c) safranal and (d) crocetin with protease (PDBID = 6M03) at entrance of lipid bilayer. The cyan, white and red vdW spheres show the carbon, hydrogen and oxygen atoms in drug molecules, respectively. The main protease is shown with white, green, red and blue cartoon which represent nonpolar, polar, acidic and basic amino acids, respectively.

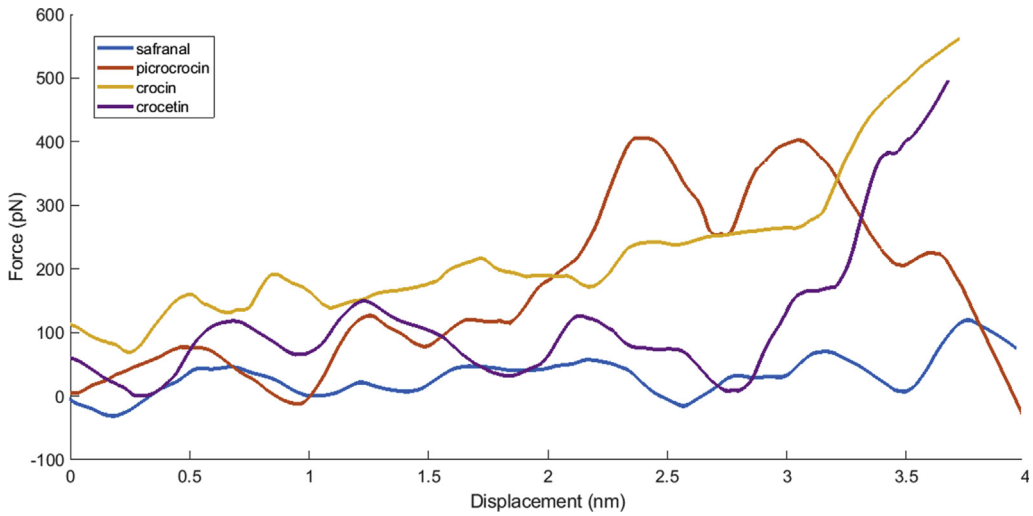

Figure 12. The force-displacement profile of drug molecules during binding to main protease (PDB ID = 6M03) of SARS-CoV-2.

Supplementary video related to this article can be found at https://doi.org/10.1016/j.heliyon.2020.e05681

The interaction site of drug molecules with the spike protein at entrance of lipid bilayer is represented in Figure 4. It is clear that the drug molecules have different interaction sites which is depicted with more detail in Figure 5. The picrocrocin dug molecule placed in a position towards the spike protein which polar atoms of picrocrocin are in adjacent with polar and basic amino acids (Figure 5 (a)). As it is illustrated in Figure 5(b) the polar groups (oxygen atoms) of the crocin drug molecule are in adjacent with polar and basic amino acids of the spike protein whereas the nonpolar atoms of picrocrocin (carbon chain) are not very close to the spike protein it seems the non-polar part of crocin drug molecule incline towards hydrophobic part of lipid bilayer. Figure 5 (c) elucidates that the safranal drug molecule positioned at a larger distance from the spike protein in comparison with three other drug molecules. As it is depicted in Figure 5(d) the crocetin drug molecule interacts with polar and acidic amino acids of the spike protein.

The Lennard-Jones (LJ) and electrostatic potentials between drug molecules and lipid bilayer were calculated to reveal the penetration mechanism of drug molecules. The LJ potential between drug molecules and spike protein and DPPC bilayer are represented in Figure. 6 (a) and Figure. 6(b), respectively. As it is demonstrated in Figure 6, when the drug molecules are placed in a distance of 4 nm from the center of mass of lipid bilayer (zero displacement), there is no LJ interaction between drug molecules and spike protein and DMPC lipid bilayer. By approaching drug molecules to lipid bilayer the LJ potential increased, which is similar to previous studies [68]. The membrane region is defined with dash lines in Figure 6. The negative values of LJ potential verify the attraction force between drug molecules and lipid bilayer [69]. Figure 6(a) clarifies that the picrocrocin does not have a significant LJ interaction with spike protein. When the crocin and crocetin drug molecules entered lipid bilayer their LJ potential with spike protein increased to -160 kJ/mol. Whereas the maximum LJ potential between the safranal and spike protein is -80 kJ/mol which confirms Figure 5 (c) where safranal drug molecule placed at more distance towards the spike protein and LJ and vdW potential are inversely proportional with distance [70]. Then the drug molecules continued their pass and by exiting them from lipid bilayer the LJ potential decreased. The trend of LJ potential between drug molecules and DPPC lipid bilayer in Figure 6 (b) is similar to Figure 6(a). High LJ potential between the crocin drug molecule and DPPC bilayer is demonstrated in Figure 6 (b) this high potential of interaction could interpret the extraction of lipid molecule which was observed in Figure. S4 (d) and Figure 5 (b).

The electrostatic potential between drug molecules and spike protein and DPPC bilayer are depicted in Figure. 7 (a) and Figure. 7 (b), respectively. The electrostatic potential between drug molecules and spike protein and DPPC lipid bilayer is not notable in the out of membrane region. Figure 7 (a) indicates that the safranal drug molecule does not have remarkable electrostatic interaction with spike protein. the picrocrocin drug molecule showed -115 kJ/mol electrostatic interaction with spike protein in the entrance of lipid bilayer but it was instantaneous and dropped fast. On the other hand, there is a strong electrostatic interaction between crocin and crocetin and spike protein in the membrane region. As it is demonstrated in Figure 7 (b), the electrostatic interactions between drug molecules and DPPC lipid bilayer is considerable in the entrance and outlet of lipid bilayer where hydrophilic groups are present while due to the hydrophobic nature of the center of lipid bilayer a decline in electrostatic potential was observed. The safranal drug molecule has a weak electrostatic interaction with DPPC lipid bilayer. The crocetin and picrocrocin have electrostatic interaction with polar groups (head groups) of DPPC whereas the crocin drug molecule has strong electrostatic interaction with DPPC that could justify the reason for extracting lipid in Figure. S5(d). The number of hydrogen bonds between the drug molecules and spike protein is described in Figure 8. It is explained in Figure 8 where the electrostatic between drug molecules and spike protein increase, the number of hydrogen bonds between them is high. the safranal drug molecule has the minimum electrostatic potential and number of hydrogen bonds with spike protein. The crocin and crocetin have maximum electrostatic potential and hydrogen bond with spike protein.

The force of translocation of drug molecules versus displacement is illustrated in Figure 9. As it is depicted in Figure 9, when the drug molecules entered the membrane region, the force increased. This increase in force is due to LJ and electrostatic potentials (Figure.4 and Figure. 5). The pulling force increased until the drug molecule reached the centre of the lipid bilayer, where the maximum value of pulling force was observed. Then the drug molecule continued its way and in the exit path, the force decreased gradually this trend in force profile also was observed in similar studies [71,72,73]. The maximum point in force-displacement profiles identifies the binding energy between the drug molecule and the lipid bilayer [74]. The results in Figure 7 prove that the crocetin drug molecule has the highest binding affinity with the lipid bilayer which is in accordance with QM calculations that showed the crocetin has strong dipole moment which facilitates penetration of

drug through lipid bilayer. This result also obtained in other studied where drugs with higher dipole moment have more tendency to encapsulate in drug carriers [75].

3.4. Binding to main protease

Initially the drug molecules were placed at a distance of 5 nm from the center of mass of the main protease. Then they pulled towards main protease with a constant velocity as it is illustrated in Figure S6 (see also Videos S5, S6, S7 and S8). The interaction sites of drug molecules on the surface of the main protease is illustrated in Figure 10. The different properties of drug molecules caused the diverse interaction sites for them. As it is depicted in Figure 11 (a) the oxygen atoms of picrocrocin positioned in a place near to glutamic (GLU) amino acid which is acidic. Figure 11 (b) elucidates that the non-polar atoms of crocin molecule (carbon chain) placed near to alanine (ALA), phenylalanine (PHE), methionine (MET) and proline (PRO) which are nonpolar amino acids. Also the polar atoms of crocin are near to serine (SER) as polar amino acid and arginine (ARG) and lysine (LYS) as basic amino acids. The interaction site of safranal is same as crocin but the distance between crocin and main protease in lower than the distance between safranal and main protease. The crocetin drug molecule (Figure 11 (d)) interacts with polar and acidic amino acids which are threonine (THR) and aspartic acid (ASP), respectively.

Supplementary video related to this article can be found at https://doi.org/10.1016/j.heliyon.2020.e05681

The force-displacement profile of drug molecules during binding to the main protease is shown in Figure 12. There is no strong force between the safranal and the main protease. When the picrocrocin was placed at the distance of 2.5 nm (2.5 nm displacement) from the main protease a maximum in force profile was observed. On the other hand, the maximum force of crocin and crocetin appeared at.

at distance 1.5 nm (3.5 nm displacement) from the main protease. The difference in location of maximum force ascertains that picrocrocin bound to a site of protease which is different from crocin and crocetin. The LJ and electrostatic potential and the number of hydrogen bonds between drug molecules and the main protease of SARA-CoV-2 are presented in Figure. S7, Figure. S8 and Figure. S9, respectively. The safranal drug molecule does not have noticeable LJ and electrostatic interactions with the main protease. The maximum LJ and electrostatic potential of picrocrocin were observed at distance 2.5 nm from the main protease where the pulling force is maximum. Also, these mentioned maximum interactions were observed at the distance of 1.5 nm from the main protease for crocin and picrocrocin. The value of maximum force, which is equivalent to binding energy, for crocin and crocetin was higher than the other two drugs.

4. Conclusion

In this study by employing steered molecular dynamics, as a powerful and efficient method, the binding affinity between main components of saffron that include: crocin, crocetin, safranal, and picrocrocin as drug molecules and spike protein and main protease of SARS-CoV-2 was evaluated. At first, the spike protein embedded in a 128 DPPC bilayer and translocation of drug molecules through this lipid bilayer was simulated. The Lennard-Jones and electrostatic potential and formation of hydrogen bonds between drug molecules and protein were recognized. The obtained force-displacement profile proved that crocetin has the maximum force and so maximum binding affinity to spike protein. The pharmacokinetic and toxicological parameters indicated that crocetin has high drug score and satisfies rules of five. Also, the obtained results from QM calculations elucidated that the strong dipole moment and polarizability of crocetin drug molecules facilitates drug penetration through lipid bilayer. In the next step binding between drug molecules and the main protease of SARS-CoV-2 was determined. The interaction sites of drug molecules with spike protein and main protease which are depicted with detail in Figure. 5 and Figure. 11, showed that the drug molecules have special interaction site with proteins that are controlled by their functional groups. The obtained result elucidated that crocin and crocetin drug molecules have a high binding affinity towards the main protease. Crocetin is the drug molecule that has a good translocation from lipid bilayer and a high binding affinity to the main protease. This study by considering spike protein and main protease tried to represent a complete representation of SARS-CoV-2 which could be a promising tool for finding treatments.

Declarations

Author contribution statement

A.R. Saadatabadi: Conceived and designed the experiments; Analyzed and interpreted the data.

A. Kordzadeh: Performed the experiments; Wrote the paper.

A. Hadi: Contributed reagents, materials, analysis tools or data.

Funding statement

This research did not receive any specific grant from funding agencies in the public, commercial, or not-for-profit sectors.

Data availability statement

Data will be made available on request.

Competing interest statement

The authors declare no conflict of interest.

Additional information

Supplementary content related to this article has been published online at https://doi.org/10.1016/j.heliyon.2020.e05681.

References

[1] D.S. Hui, E.I. Azhar, T.A. Madani, F. Ntoumi, R. Kock, O. Dar, G. Ippolito, T.D. Mchugh, Z.A. Memish, C. Drosten, The continuing 2019-nCoV epidemic threat of novel coronaviruses to global health—the latest 2019 novel coronavirus outbreak in Wuhan, China, Int. J. Infect. Dis. 91 (2020) 264.

[2] I.I. Bogoch, A. Watts, A. Thomas-Bachli, C. Huber, M.U.G. Kraemer, K. Khan, Pneumonia of unknown aetiology in Wuhan, China: potential for international spread via commercial air travel, J. Trav. Med. (2020). **27**taaa008.

[3] Q. Tang, Y. Song, M. Shi, Y. Cheng, W. Zhang, X.-Q. Xia, Inferring the hosts of coronavirus using dual statistical models based on nucleotide composition, Sci. Rep. 5 (2015) 17155.

[4] P.C.Y. Woo, Y. Huang, S.K.P. Lau, K.-Y. Yuen, Coronavirus Genomics and Bioinformatics Analysis *Viruses* **2** 1804–20, 2010.

[5] J. Cui, F. Li, Z.-L. Shi, Origin and evolution of pathogenic coronaviruses, Nat. Rev. Microbiol. 17 (2019) 181–192.

[6] N. Zhu, D. Zhang, W. Wang, X. Li, B. Yang, J. Song, X. Zhao, B. Huang, W. Shi, R. Lu, A novel coronavirus from patients with pneumonia in China, 2019, N. Engl. J. Med. (2020).

[7] Zhang L, Shen F M, Chen F and Lin Z 3AD February 2020, posting date Origin and evolution of the 2019 novel coronavirus Clin. Infect. Dis. **10**

[8] W.H. Organization, WHO COVID-19 Essential Supplies Forecasting Tool (COVID-19-Esft): Frequently Asked Questions (FAQ), 24 April 2020, World Health Organization), 2020.

[9] Y. Muhammed, Biosafety and Health Molecular Targets for COVID-19 Drug Development : Enlightening Nigerians about the Pandemic and Future Treatment *Biosaf*, Heal, 2020.

[10] C. Gil, T. Ginex, I. Maestro, V. Nozal, L. Barrado-gil, -M.A. Cuesta, J. Urquiza, D. Ramírez, C. Alonso, N.E. Campillo, A. Martínez, COVID-19 : drug targets and potential treatments COVID-19 : drug targets and potential treatments, 2020.

[11] K. Stadler, V. Masignani, M. Eickmann, S. Becker, S. Abrignani, H.-D. Klenk, R. Rappuoli, SARS—beginning to understand a new virus, Nat. Rev. Microbiol. 1 (2003) 209–218.

[12] P. Zhou, X.L. Yang, X.G. Wang, B. Hu, L. Zhang, W. Zhang, H.R. Si, Y. Zhu, B. Li, C.L. Huang, Discovery of a novel coronavirus associated with the recent pneumonia outbreak in humans and its potential bat origin, bioRxiv *Cold Spring Harb Lab* 2020 (2020) 22–914952.

[13] P. Adhikari, N. Li, M. Shin, N.F. Steinmetz, R. Twarock, R. Podgornik, W.-Y. Ching, Intra-and intermolecular atomic-scale interactions in the receptor binding domain of SARS-CoV-2 spike protein: implication for ACE2 receptor binding, Phys. Chem. Chem. Phys. (2020).

[14] K. Swiderek, V. Moliner, Revealing the Molecular Mechanisms of Proteolysis of SARS-CoV-2 Mpro from QM/MM Computational Methods, 2020.

[15] A.I. Owis, M.S. El-Hawary, D. El Amir, O.M. Aly, U.R. Abdelmohsen, M.S. Kamel, Molecular docking reveals the potential of Salvadora persica flavonoids to inhibit COVID-19 virus main protease, RSC Adv. 10 (2020) 19570–19575.

[16] P. Procacci, M. Macchiagodena, M. Pagliai, G. Guarnieri, F. Iannone, Interaction of Hydroxychloroquine with SARS-CoV2 Functional Proteins Using All-Atoms Non-equilibrium Alchemical Simulations, 2020.

[17] A.A. Elfiky, Anti-HCV, Nucleotide Inhibitors, Repurposing against COVID-19, Life sciences, 2020, p. 117477.

[18] S. Bharadwaj, K.E. Lee, V.D. Dwivedi, S.G. Kang, Computational Insights into Tetracyclines as Inhibitors against SARS-CoV-2 Mpro via Combinatorial Molecular Simulation Calculations, Life Sci. 257 (2020) 118080.

[19] A. Sethi, S. Sanam, S. Munagalasetty, S. Jayanthi, M. Alvala, Understanding the role of galectin inhibitors as potential candidates for SARS-CoV-2 spike protein: in silico studies, RSC Adv. 10 (2020) 29873–29884.

[20] A. Góra, Molecular Dynamics Simulations Indicate the COVID-19 Mpro Is Not a Viable Target for Small-Molecule Inhibitors Design, 2020.

[21] I. Aanouz, A. Belhassan, T. Lakhlifi, Moroccan Medicinal plants as inhibitors against SARS-CoV-2 main protease : computational investigations Moroccan Medicinal plants as inhibitors against SARS-CoV-2 main protease : computational investigations, *J. Biomol. Struct. Dyn.* **0** 1–9 (2020).

[22] I. Franc, A. Lipinski, P.J. Feeney, Experimental and Computational Approaches to Estimate Solubility and Permeability in Drug Discovery and Development Settings **23**, 1997.

[23] C.A.L. Ã, Lead Profiling Lead- and Drug-like Compounds : the Rule-Of-Five Revolution 337–41, 2004.

[24] K.P. Ravindranathan, V. Mandiyan, A.R. Ekkati, J.H. Bae, J. Schlessinger, W.L. Jorgensen, Discovery of novel fibroblast growth factor receptor 1 kinase inhibitors by structure-based virtual screening, J. Med. Chem. 53 (2010) 1662–1672.

[25] J. Åqvist, C. Medina, J.-E. Samuelsson, A new method for predicting binding affinity in computer-aided drug design *Protein*, Eng. Des. Sel. 7 (1994) 385–391.

[26] H. Grubmüller, B. Heymann, P. Tavan, Ligand binding: molecular mechanics calculation of the streptavidin-biotin rupture force *Science* 80 (1996) 997–999, 271.

[27] B. Isralewitz, M. Gao, K. Schulten, Steered molecular dynamics and mechanical functions of proteins, Curr. Opin. Struct. Biol. 11 (2001) 224–230.

[28] H. Lu, B. Isralewitz, A. Krammer, V. Vogel, K. Schulten, Unfolding of titin immunoglobulin domains by steered molecular dynamics simulation, Biophys. J. 75 (1998) 662–671.

[29] B. Isralewitz, J. Baudry, J. Gullingsrud, D. Kosztin, K. Schulten, Steered molecular dynamics investigations of protein function, J. Mol. Graph. Model. 19 (2001) 13–25.

[30] T. Giorgino, G. De Fabritiis, A high-throughput steered molecular dynamics study on the free energy profile of ion permeation through Gramicidin, J. Chem. Theor. Comput. 7 (2011) 1943–1950.

[31] J.-F. Gwan, A. Baumgaertner, Cooperative transport in a potassium ion channel, *J. Chem. Phys.* **127**07B616 (2007).

[32] M.Ø. Jensen, S. Park, E. Tajkhorshid, K. Schulten, Energetics of glycerol conduction through aquaglyceroporin GlpF, Proc. Natl. Acad. Sci. Unit. States Am. 99 (2002) 6731–6736.

[33] J. Hénin, E. Tajkhorshid, K. Schulten, C. Chipot, Diffusion of glycerol through Escherichia coli aquaglyceroporin GlpF *Biophys*, J 94 (2008) 832–839.

[34] L. Shen, J. Shen, X. Luo, F. Cheng, Y. Xu, K. Chen, E. Arnold, J. Ding, H. Jiang, Steered molecular dynamics simulation on the binding of NNRTI to HIV-1 RT, Biophys. J. 84 (2003) 3547–3563.

[35] Y. Xu, J. Shen, X. Luo, I. Silman, J.L. Sussman, K. Chen, H. Jiang, How does huperzine A enter and leave the binding gorge of acetylcholinesterase? Steered molecular dynamics simulations, J. Am. Chem. Soc. 125 (2003) 11340–11349.

[36] L. Le, E.H. Lee, D.J. Hardy, T.N. Truong, K. Schulten, Molecular dynamics simulations suggest that electrostatic funnel directs binding of Tamiflu to influenza N1 neuraminidases *PLoS*, Comput Biol 6 (2010), e1000939.

[37] T. Rungrotmongkol, P. Yotmanee, N. Nunthaboot, S. Hannongbua, Computational studies of influenza A virus at three important targets: hemagglutinin, neuraminidase and M2 protein, Curr. Pharmaceut. Des. 17 (2011) 1720–1739.

[38] B.K. Mai, M.H. Viet, M.S. Li, Top leads for swine influenza A/H1N1 virus revealed by steered molecular dynamics approach, J. Chem. Inf. Model. 50 (2010) 2236–2247.

[39] J. Srinivasan, T.E. Cheatham, P. Cieplak, P.A. Kollman, D.A. Case, Continuum solvent studies of the stability of DNA, RNA, and phosphoramidate− DNA helices, J. Am. Chem. Soc. 120 (1998) 9401–9409.

[40] P.A. Kollman, I. Massova, C. Reyes, B. Kuhn, S. Huo, L. Chong, M. Lee, T. Lee, Y. Duan, W. Wang, Calculating structures and free energies of complex molecules: combining molecular mechanics and continuum models, Acc. Chem. Res. 33 (2000) 889–897.

[41] D.C. Garc-Olmo, H.H. Riese, J. Escribano, n J. Ontã́, J.A. Fernandez, M. Atiénzar, D. Garcí-Olmo, Effects of long-term treatment of colon adenocarcinoma with crocin, a carotenoid from saffron (Crocus sativus L.): an experimental study in the rat, Nutr. Canc. 35 (1999) 120–126.

[42] M.J. Gregory, R.C. Menary, N.W. Davies, Effect of drying temperature and air flow on the production and retention of secondary metabolites in saffron, J. Agric. Food Chem. 53 (2005) 5969–5975.

[43] F. Hadizadeh, N. Khalili, H. Hosseinzadeh, R. Khair-Aldine, Kaempferol from saffron petals, Chem. Prepr. Arch. 2003 (2003) 234–239.

[44] S. Soleymani, R. Zabihollahi, S. Shahbazi, A. Bolhassani, Antiviral effects of saffron and its major ingredients, Curr. Drug Deliv. 15 (2018) 698–704.

[45] J. Escribano, G.-L. Alonso, M. Coca-Prados, J.-A. Fernández, Crocin, safranal and picrocrocin from saffron (Crocus sativus L.) inhibit the growth of human cancer cells in vitro *Cancer*, Lettres (1996) **100** 23–30.

[46] www.immunology.org/public-information/bitesized-immunology/pathogens-and-disease/viruses-introduction.

[47] www.wikipedia.org.

[48] www.drugbank.ca.

[49] S.K. Burley, H.M. Berman, C. Bhikadiya, C. Bi, L. Chen, L. Di Costanzo, C. Christie, K. Dalenberg, J.M. Duarte, S. Dutta, RCSB Protein Data Bank: biological macromolecular structures enabling research and education in fundamental biology, biomedicine, biotechnology and energy, Nucleic Acids Res. 47 (2019) D464–D474.

[50] www.charmm-gui.org/?doc=input/membrane.bilayer charmm-gui.

[51] J.F. Nagle, Area/lipid of bilayers from NMR, Biophys. J. 64 (1993) 1476–1481.

[52] D. Van Der Spoel, E. Lindahl, B. Hess, G. Groenhof, A.E. Mark, H.J.C. Berendsen, GROMACS: fast, flexible, and free, J. Comput. Chem. 26 (2005) 1701–1718.

[53] W. Humphrey, A. Dalke, K. Schulten, VMD: visual molecular dynamics, J. Mol. Graph. 14 (1996) 33–38.

[54] N. Schmid, A.P. Eichenberger, A. Choutko, S. Riniker, M. Winger, A.E. Mark, W.F. van Gunsteren, Definition and testing of the GROMOS force-field versions 54A7 and 54B7, Eur. Biophys. J. 40 (2011) 843.

[55] H.J.C. Berendsen, J.P.M. Postma, W.F. van Gunsteren, J. Hermans, Interaction Models for Water in Relation to Protein Hydration *Intermolecular Forces*, Springer, 1981, pp. 331–342.

[56] Pdavapc1.bioch.dundee.ac.uk/cgi-bin/prodrg/.

[57] B.M. Bode, M.S. Gordon, MacMolPlt: a graphical user interface for GAMESS, J. Mol. Graph. Model. 16 (1998) 133–138.

[58] A.D. Becke, Density-functional thermochemistry. III. The role of exact exchange, J. Chem. Phys. 98 (1993) 5648–5652.

[59] M.W. Schmidt, K.K. Baldridge, J.A. Boatz, S.T. Elbert, M.S. Gordon, J.H. Jensen, S. Koseki, N. Matsunaga, K.A. Nguyen, S. Su, General atomic and molecular electronic structure system, J.Comput. Chem. 14 (1993) 1347–1363.

[60] V. Mironov, Y. Alexeev, D.G. Fedorov, MPI/OpenMP Parallelization of the Fragment Molecular Orbitals Method in GAMESS *Google Sch. There Is No Corresp. Rec. This Ref*, 2018.

[61] www.swissadme.ch/index.php.

[62] G. Bussi, D. Donadio, M. Parrinello, Canonical sampling through velocity rescaling, J. Chem. Phys. 126 (2007) 14101.

[63] H.J.C. Berendsen, Postma J P M van, W.F. van Gunsteren, A. DiNola, J.R. Haak, Molecular dynamics with coupling to an external bath, J. Chem. Phys. 81 (1984) 3684–3690.

[64] A. Yousefpour, S. Amjad Iranagh, Y. Nademi, H. Modarress, Molecular dynamics simulation of nonsteroidal antiinflammatory drugs, naproxen and relafen, in a lipid bilayer membrane, Int. J. Quant. Chem. 113 (2013) 1919–1930.

[65] H. Zheng, B. Wang, Y. Wu, Molecular dynamics simulation on the interfacial features of phenol extraction by TBP/dodecane in water, Comput. Theor. Chem. 970 (2011) 66–72.

[66] T. Darden, D. York, L. Pedersen, Particle mesh Ewald: an N· log (N) method for Ewald sums in large systems, J. Chem. Phys. 98 (1993) 10089–10092.

[67] G. Sutmann, Classical molecular dynamics, Quantum simulations complex many-body Syst. from theory to algorithms 10 (2002) 211–254.

[68] S.Z. Mousavi, S. Amjad-Iranagh, Y. Nademi, H. Modarress, Carbon nanotube-encapsulated drug penetration through the cell membrane: an investigation based on steered molecular dynamics simulation, J. Membr. Biol. 246 (2013) 697–704.

[69] Shi S, Strength A and Gopakumar S T CHEN 7200/7206–Chemical Engineering Thermodynamics

[70] J.M. Prausnitz, R.N. Lichtenthaler, E.G. De Azevedo, Molecular Thermodynamics of Fluid-phase Equilibria, Pearson Education), 1998.

[71] S. Vemparala, L. Saiz, R.G. Eckenhoff, M.L. Klein, Partitioning of anesthetics into a lipid bilayer and their interaction with membrane-bound peptide bundles, Biophys. J. 91 (2006) 2815–2825.

[72] V.K. Gangupomu, F.M. Capaldi, Interactions of carbon nanotube with lipid bilayer membranes, X Bai *J. Nanomater.* 2011 (2011) 830436.

[73] E.J. Wallace, M.S.P. Sansom, Blocking of carbon nanotube based nanoinjectors by lipids: a simulation study, Nano Lett. 8 (2008) 2751–2756.

[74] M.S. Li, B.K. Mai, Steered Molecular Dynamics- $ Promising Tool for Drug Design, 2012, pp. 342–351.

[75] A. Kordzadeh, S. Amjad-Iranagh, M. Zarif, H. Modarress, Adsorption and encapsulation of the drug doxorubicin on covalent functionalized carbon nanotubes: a scrutinized study by using molecular dynamics simulation and quantum mechanics calculation, J. Mol. Graph. Model. 88 (2019) 11–22.